The Journal of Immunology

RESEARCH ARTICLE | MARCH 22 2023

Epidermal Growth Factor Receptor in Hepatic Endothelial Cells Suppresses MCP-1–Dependent Monocyte Recruitment in Diabetes FREE

Xinyi Zhang; ... et. al

J Immunol (2023) 210 (9): 1363–1371.
https://doi.org/10.4049/jimmunol.2200557

Epidermal Growth Factor Receptor in Hepatic Endothelial Cells Suppresses MCP-1–Dependent Monocyte Recruitment in Diabetes

Xinyi Zhang,*[,1] Lee Ohayon-Steckel,[†,‡,1] Emilie Coppin,[§,¶] Ebin Johny,[†] Ankush Dasari,[†] Jonathan Florentin,[†] Sathish Vasamsetti,[†] and Partha Dutta[†,‡,‖,#,**]

Insulin resistance is a compromised response to insulin in target tissues such as liver. Emerging evidence shows that vascular endothelial cells (ECs) are critical in mediating glucose metabolism. However, how liver ECs can regulate inflammation in the setting of insulin resistance is still unknown. Using genome-wide transcriptome analysis of ECs isolated from diabetic mice, we found enrichment of the genes involved in epidermal growth factor receptor (Egfr) signaling. In line with this, hepatic sinusoidal ECs in diabetic mice had elevated levels of Egfr expression. Interestingly, we found an increased number of hepatic myeloid cells, especially macrophages, and systemic glucose intolerance in *Cdh5*$^{Cre/+}$*Egfr*$^{fl/fl}$ mice lacking *Egfr* in ECs compared with littermate control mice with type II diabetes. Egfr deficiency upregulated the expression of MCP-1 in hepatic sinusoidal ECs. This resulted in augmented monocyte recruitment and macrophage differentiation in *Cdh5*$^{Cre/+}$*Egfr*$^{fl/fl}$ mice compared with littermate control mice as determined by a mouse model of parabiosis. Finally, MCP-1 neutralization and hepatic macrophage depletion in *Cdh5*$^{Cre/+}$*Egfr*$^{fl/fl}$ mice resulted in a reduced number of hepatic macrophages and ameliorated glucose intolerance compared with the control groups. Collectively, these results demonstrate a protective endothelial Egfr signaling in reducing monocyte-mediated hepatic inflammation and glucose intolerance in type II diabetic mice. ***The Journal of Immunology*****, 2023, 210: 1363–1371.**

Type II diabetes is an expanding global public health issue and has gradually become a financial burden to society. The International Diabetes Federation reported that, in 2021, ~537 million adults (20–79 y) worldwide were living with diabetes, and 79% of them were from low/middle-income countries. This number is expected to increase to 783 million by 2045 (1). The impaired glucose homeostasis leads to hyperglycemia in diabetic patients, as well as the dysregulation of carbohydrate, lipid, and protein metabolism. Chronic hyperglycemia also contributes to the development of microvascular complications in various organs, including the eyes, kidneys, and brain, and macrovascular complications, such as myocardial infarction, peripheral vascular disease, and other cardiovascular diseases (2, 3).

Both genetic and environmental factors promote the pathogenesis of type II diabetes and its complications, resulting in multiple pathophysiological abnormalities that are responsible for weakened insulin secretion, insulin resistance, or a combination of both (4). Among these factors, the activation of inflammatory pathways can induce chronic and systemic inflammation, closely linked to insulin resistance. High levels of proinflammatory cytokines, such as IL-6 and TNF, and augmented quantities of macrophages, along with other inflammatory cells, are found in adipose tissue and livers of diabetic patients and animals (4, 5). Proinflammatory cytokines are able to trigger insulin resistance via activating downstream kinases, including MAPK, IκB kinase-β, and JNK1, which further hamper the insulin signal transduction pathway (4, 6, 7). Other signaling, including reactive oxygen species, advanced glycation end products, and advanced glycation end product receptors, has also been proven to be involved in the activation of several proinflammatory pathways and the induction of diabetic complications (8, 9).

Besides, macrophage infiltration is another crucial contributor to insulin resistance (10). In adipose tissue in obesity, there is an expansion of proinflammatory macrophages, Th17, and CD8$^+$ T cells and a decrease in the numbers of anti-inflammatory macrophages and

*Department of Cardiology, Second Affiliated Hospital of Zhejiang University School of Medicine, Hangzhou, China; [†]Pittsburgh Heart, Lung, Blood, and Vascular Medicine Institute, University of Pittsburgh, Pittsburgh, PA; [‡]Department of Bioengineering, Swanson School of Engineering, University of Pittsburgh, Pittsburgh, PA; [§]Regeneration in Hematopoiesis, Institute for Immunology, TU Dresden, Dresden, Germany; [¶]Immunology of Aging, Leibniz Institute on Aging–Fritz Lipmann Institute, Jena, Germany; [‖]Division of Cardiology, Department of Medicine, University of Pittsburgh, Pittsburgh, PA; [#]Department of Immunology, University of Pittsburgh School of Medicine, Pittsburgh, PA; and **Pittsburgh VA Medical Center-University Drive, University Drive C, Pittsburgh, PA

Received for publication July 29, 2022. Accepted for publication February 27, 2023.

[1]X.Z. and L.O.-S. contributed equally to this work.

ORCIDs: 0000-0002-5846-337X (X.Z.); 0000-0002-8857-9357 (E.J.); 0000-0003-3042-5731 (A. D.); 0000-0001-7481-4128 (J.F.); 0000-0002-9682-7437 (S.V.); 0000-0001-7456-1757 (P.D.).

This work was supported by the National Heart, Lung, and Blood Institute, National Institutes of Health (NIH; Grants R00HL121076-03, R01HL142629, and R01HL143967); NIH (Grant R01AG069399); National Institute of Diabetes and Digestive and Kidney Diseases, NIH (Grant R01DK129339); AHA Transformational Project Award (19TPA34910142); American Heart Association Innovative Project Award (19IPLOI34760566); American Lung Association Innovation Project Award (IA-629694 to P.D.); and Young Scientists Fund of the National Natural Science Foundation of China (82100346 to X.Z.). Confocal and intravital microscopy was performed using the NIH-supported microscopy resources at the Center for Biologic Imaging. Specifically, the confocal microscope was supported by NIH Grant 1S10OD019973-01. The figures were designed using BioRender software.

X.Z. and L.O.-A. designed and performed experiments, analyzed data, and wrote the manuscript. E.C. performed experiments. E.J., A.D., J.F., and S.V. helped with the technical aspects of the experiments. P.D. designed experiments, wrote the manuscript, and provided the funding to complete the study.

Address correspondence and reprint requests to Dr. Partha Dutta, Departments of Medicine and Immunology, Center for Pulmonary Vascular Biology and Medicine, Pittsburgh Heart, Lung, Blood, and Vascular Medicine Institute, University of Pittsburgh School of Medicine, 200 Lothrop Street BST1720.1, Pittsburgh, PA 15213. E-mail address: duttapa@pitt.edu

The online version of this article contains supplemental material.

Abbreviations used in this article: EC, endothelial cell; Egfr, epidermal growth factor receptor; $GdCl_3$, gadolinium chloride; GTT, glucose tolerance test; ITT, insulin tolerance test; VAT, visceral adipose tissue.

regulatory T cells (11–13). Macrophage infiltration induces lipolysis and creates an inflammatory environment in adipose tissue. Subsequently, the heightened levels of IL-6 can stimulate hepatic gluconeogenesis, and a high level of hepatic acetyl CoA can trigger hepatic insulin resistance (14).

Recent studies have underscored the significance of hepatic inflammation mediated by Kupffer cells and hepatic stellate cells in insulin resistance. These are not only target cells that respond to hyperglycemia or hyperinsulinemia but also effector cells that exacerbate insulin resistance in hepatocytes by increasing oxidative stress, altering adipocytokine balance, and secreting proinflammatory cytokines such as TNF and IL-6 (15). Endothelial cells (ECs) suffer from progressive damage in type II diabetes, leading to endothelial dysfunction (16, 17). However, it is relatively unknown how changes in hepatic sinusoidal ECs increase inflammation and insulin resistance.

The literature shows that ECs (18), macrophages (19), vascular smooth muscle cells (20), and cardiomyocytes (21) express high levels of epidermal growth factor receptor (Egfr). The activation of Egfr signaling has been found to be involved in multiple biological processes, including stimulation of cell proliferation, differentiation, and migration, and inhibition of apoptosis (22). Especially, upregulation of Egfr signaling can mediate cellular senescence induced by certain proinflammatory cytokines (23) and also strengthen innate immunity against viral infections (24). Egfr and its downstream proteins are widely used as therapeutic targets in the setting of cancer (25). In addition, studies have demonstrated that Egfr signaling is linked with cellular metabolism like glycolysis (26). Egfr transactivation by high glucose levels causes multicellular dysfunction, which promotes the development of diabetic kidney disease (27, 28).

In this study, we show that, using genome-wide transcriptome analysis, Egfr signaling increased in ECs in a mouse model of obesity. Hepatic sinusoidal ECs also had elevated expression of Egfr in these mice compared with lean mice. To understand the importance of endothelial Egfr in insulin resistance, we generated mice lacking this receptor in ECs ($Cdh5^{Cre/+}Egfr^{fl/fl}$). We observed increased glucose intolerance in these mice compared with age-matched littermate control mice ($Cdh5^{+/+}Egfr^{fl/fl}$). Sinusoidal ECs in $Cdh5^{Cre/+}Egfr^{fl/fl}$ mice produced an exaggerated amount of MCP-1, resulting in more inflammatory monocyte accumulation and Kupffer cell generation. MCP-1 neutralization and Kupffer cell depletion reversed glucose intolerance in the mice lacking *Egfr* in ECs. Taken together, our study indicates that alteration in hepatic sinusoidal ECs leads to inflammatory cell accumulation in the liver, resulting in glucose intolerance.

Materials and Methods

Mice

$Cdh5^{Cre/+}Egfr^{fl/fl}$ mice were generated and used for experiments. C57BL/6 (000664) and GFP (004353) were purchased from Jackson Laboratory. Male and female mice (12–20 wk old) were housed under specific pathogen-free conditions. All experiments, including chow and high-fat-diet feeding and parabiosis, were approved by the Institutional Animal Care and Use Committee of the University of Pittsburgh (21079629). The $Egfr^{fl/fl}$ mice were generous gifts from Dr. M. Nahrendorf (29). Cryo-derived $Egfr^{fl/fl}$ mice (B6.129S6-Egfrtm1Dwt/Mmnc, identification number: 031765-UNC, >99% C57BL/6J background) were obtained from the Mutant Mouse Resource and Research Centers (Chapel Hill, NC). $Cdh5^{cre/+}$ mice were purchased from the Jackson Laboratory (catalog number 006137) and were crossed with $Egfr^{fl/fl}$ mice to obtain EC-specific *Egfr*-deficient mice.

Type II diabetes induction

Type II diabetes was induced by an established high-fat diet. $Cdh5^{Cre/+}Egfr^{fl/fl}$ and littermate control mice were fed with a high-fat diet containing 60 kcal% fat (D12492; Research Diets) for 4 mo.

Glucose and insulin tolerance tests

Female mice were fasted for 6 h, and baseline glucose levels were measured. A 15% glucose solution was prepared using 1× PBS and D-(+)-glucose (G8270; Sigma). Mice received 2 mg glucose per gram body weight i.p. Glucose measurements were taken at 0, 15, 30, 60, 90, 120, and 150 min after injection. For insulin tolerance test (ITT), after fasting for 6 h, female mice were injected with insulin (0.25 U/kg body weight) (12-585-014; Fisher Scientific), and blood glucose concentrations were assessed at 0, 15, 30, 60, 90, and 120 min after injection.

Organ harvesting, flow cytometry, and cell sorting

Male and female mice were euthanized and perfused thoroughly with 20 ml of ice-cold PBS through the left ventricle to remove blood from solid organs. Gonadal visceral adipose tissues (VATs) from the pelvic cavity and liver were harvested and digested in PBS containing 1 mg/ml collagenase IV (LS004209; Worthington) and HEPES buffer (25-060-CI; Corning) at 37°C at 750 rpm for 1 h. Samples were then washed with 10 ml of sterile PBS and filtered through 40-μm filters. Cells were centrifuged at 350 × *g* and 4°C for 7 min. The supernatant was discarded, and cells were stained with Abs against Ly-6C (128006; BioLegend), CD64 (558455; BD Biosciences), CD115 (750887; eBioscience), F4/80 (123114; BioLegend), Ly-6G (127614; BioLegend), CD11b (557657; BD Biosciences), CD45.2 (560693; BD Biosciences), CD3 (564008; BD Biosciences), I-A/I-E (MHC class II) (107620; BioLegend), CD11c (117338; BioLegend), CD19 (563148; BD Biosciences), CD31 (102418; BioLegend), CD54/ICAM-1 (116120; BioLegend), CD106/VCAM-1 (11106181; eBioscience), and EGFR (558523; BD Biosciences). Myeloid cells were identified as $CD45.2^+CD11b^+$, and neutrophils were defined as $CD45.2^+CD11b^+Ly6G^+CD115^-$. Monocytes and Kupffer cells were considered as $CD45.2^+CD11b^+CD115^+Ly6G^-$ and $CD45.2^+CD11b^+CD115^+Ly6G^-F4/80^+CD64^+$, respectively. Ly-$6C^{hi}$ monocytes were defined as $CD45.2^+CD11b^+CD115^+Ly6G^-Ly\text{-}6C^+$, and Ly-$6C^{lo}$ monocytes were $CD45.2^+CD11b^+CD115^+Ly6G^-Ly\text{-}6C^-$. Data acquisition was performed using a Fortessa Flow Cytometer (BD). Data were analyzed using FlowJo software (Tree Star).

Microarray

The microarray method was discussed in detail previously (29). In brief, 5000 bone marrow ECs were sorted from male nondiabetic and diabetic C57BL/6J mice using FACS with >95% purity. Gene expression profiling was performed by the Partners HealthCare Personalized Medicine Translational Genomics Core. Amplified cDNA was prepared using the Ovation Pico WTA System V2 (NuGEN) and hybridized to GeneChip Mouse Gene 2.0 ST arrays (Affymetrix). The raw microarray data were normalized with the robust multiarray average, and differentially expressed genes were determined with the Bioconductor Limma package.

Immunofluorescence microscopy

Followed by euthanization of mice and PBS perfusion through the left ventricle, VAT and liver were excised and fixed with 4% buffered formalin for 2 h and stored in 30% sucrose solution containing 0.05% sodium azide for overnight. Then, the tissues were embedded in OCT blocks and cut into sections (6 μm). Samples were permeabilized with 0.1% Triton X-100 for an hour. After blocking, mouse tissue sections were stained with anti-F4/80 (MA1-91124 [Invitrogen]; MA5-16363 [Thermo Fisher]), CD11b (ab133357; Abcam), CD31/VE Cadherin (ab7388 [Abcam]; MA1-80069 [Thermo Fisher]), VCAM-1 (PA5-86042 [Invitrogen]), p-EGFR (44-794G [Invitrogen]), and MCP-1 (MA5-17040 [Invitrogen]) followed by staining with fluorochrome-conjugated secondary Abs. The sections were stained and fixed with Vectashield mounting medium with DAPI (#H 1200; Vector Laboratories), and images were taken using Nikon A1 spectral confocal for immunofluorescence scanning using 20× magnification. Livers from four to five mice per group were sectioned three times, and two images per section were taken. Image analysis was done using ImageJ software. Distance measurement of macrophages from sinusoidal ECs was performed by ImageJ by drawing straight lines from macrophages to the nearest sinusoidal EC.

In vitro transfection

Human hepatic ECs (SK-HEP-1; ATCC) were cultured in EMEM (30-2003; ATCC) containing 10% FBS and 1% penicillin and streptomycin in the presence or absence of palmitate (EW-88353-70; Cole-Parmer). The cells were transfected with 2 nM si*EGFR* (MC10516; Thermo Fisher Scientific) or control siRNA (4464058; Thermo Fisher Scientific) with Lipofectamine 11 2000 (12566014; Thermo Fisher Scientific) per the manufacturer's protocol.

Parabiosis

Postanesthesia, adjacent sides of GFP$^+$ and *Cdh5*$^{Cre/+}$*Egfr*$^{fl/fl}$ or *Cdh5*$^{+/+}$ *Egfr*$^{fl/fl}$ mice were sterilized with butadiene scrub followed by 70% isopropanol. An incision was made from the ear to the tail of each mouse. The s.c. fascia was bluntly dissected to create ~0.5 cm of free skin. The olecranon and knee joints were attached by a single 2-0 silk suture and tied. The skin of the mice was joined together using a 5-0 suture. Stifle and elbows were joined to avoid stress on the suture lines. We performed the parabiosis experiments in two cohorts of mice. The first cohort was female mice, and the second cohort was male mice.

In vivo MCP-1 neutralization

To study MCP-1 depletion, we injected i.v. 15 μg of a neutralizing Ab against mouse MCP-1 or control goat IgG (AB-108-C; R&D Systems) in female mice for 4 wk at an interval of 4 d.

In vivo hepatic macrophages deletion

To deplete hepatic macrophages, either gadolinium chloride ($GdCl_3$) (20 mg/kg per mouse; 11286; Alfa Aeser) or PBS was injected i.v. in female mice twice a week for 6 wk.

Statistics

Data are represented as mean ± SEM. Statistical significance between groups was performed using nonparametric *t* test (Mann–Whitney *U* test). Results were considered as statistically significant when $p < 0.05$. We used two-tailed nonparametric *t* test to analyze most data. However, for the area under the curve analysis in Figs. 4E, 4F, 5D, and 5H, we used one-tailed nonparametric *t* test.

Study approval

All experiments were approved by the Institutional Animal Care and Use Committee of the University of Pittsburgh.

Results

Type II diabetes alters hepatic sinusoidal ECs

To understand whether type II diabetes alters ECs in vivo, we analyzed our microarray data comparing ECs in nondiabetic and diabetic mice (29). Pathway analysis revealed that ECs in a diabetic environment are more inflammatory as indicated by upregulation of several pathways, including IFN signature, tumor field effect, and obesity (Fig. 1A). The most significantly altered pathway was EGF response. In line with this finding, we observed elevated levels of p-EGFR in hepatic sinusoidal ECs in the obese mice compared with lean mice (Fig. 1B, 1C). Consistent with this, we found increased F4/80$^+$ macrophage numbers near sinusoidal CD31$^+$ VE-cadherin$^+$ ECs in the obese mice compared with the lean control (Fig. 1D, Supplemental Fig. 1).

EC-specific Egfr *deletion enhances glucose intolerance and hepatic monocyte recruitment*

To investigate the role of endothelial Egfr in insulin resistance, we generated mice lacking this receptor in liver ECs (*Cdh5*$^{Cre/+}$*Egfr*$^{fl/fl}$) (Supplemental Fig. 2A, 2B). At baseline, glucose tolerance tests (GTTs) remained unchanged between *Cdh5*$^{Cre/+}$*Egfr*$^{fl/fl}$ and age-matched littermate control mice that were fed with regular chow diet (Supplemental Fig. 2C). Interestingly, when fed with a high-fat diet (Fig. 2A), we observed elevated glucose intolerance in the mice lacking endothelial *Egfr* when compared with littermate controls, but their body weights were similar (Fig. 2B, Supplemental Fig. 2D, 2E), indicating that endothelial Egfr signaling is crucial to glucose tolerance in the setting of type II diabetes. It has been shown that the impairment of insulin action is associated with liver and adipose tissue inflammation in obese subjects (30). To determine whether the exacerbated glucose intolerance in *Cdh5*$^{Cre/+}$*Egfr*$^{fl/fl}$ mice after feeding with a high-fat diet is indeed a result of inflammation, we enumerated leukocytes in the liver and VAT of *Cdh5*$^{Cre/+}$*Egfr*$^{fl/fl}$ and control mice that were fed with a high-fat diet for 4 mo by flow cytometry. Myeloid cells, especially macrophages, were more numerous in the liver of diabetic *Cdh5*$^{Cre/+}$*Egfr*$^{fl/fl}$ mice (Fig. 2C–E). Consistent with this, we found increased macrophage numbers near hepatic sinusoidal ECs, indicating their higher recruitment in diabetic *Cdh5*$^{Cre/+}$*Egfr*$^{fl/fl}$ mice (Fig. 2E). Conversely, the levels of myeloid cells did not differ in VAT between these two groups (Supplemental Fig. 3A). Confocal microscopy confirmed that the percentages of F4/80$^+$ macrophages and Ly6G$^+$ neutrophils in VAT were unaltered (Supplemental Fig. 3B). Collectively, these data imply that increased Egfr expression by ECs of diabetic mice suppresses hepatic inflammation and promotes glucose tolerance.

Disrupted endothelial Egfr signaling promotes monocyte recruitment via MCP-1

Monocytes can immediately respond to an alteration of tissue homeostasis and be recruited into injured tissues to differentiate into macrophages (31). Increased macrophage abundance in the liver of obese *Cdh5*$^{Cre/+}$*Egfr*$^{fl/fl}$ mice indicates accelerated differentiation of recruited monocytes in the liver. Moreover, we found these macrophages are close to hepatic sinusoidal ECs. Because hepatic sinusoids are the entry ports of inflammatory cells, and bone marrow ECs facilitate monocyte emigration after LPS treatment (32), we hypothesize that *Egfr* deficiency in hepatic ECs expediates monocyte recruitment and differentiation into macrophages. To investigate this possibility, we first quantified MCP-1, which has been widely reported to be a vital modulator of monocyte–endothelial interactions under flow conditions via triggering rolling monocytes to adhere firmly onto monolayers (33). We observed elevated MCP-1 production in hepatic ECs, but not in monocytes, of diabetic *Cdh5*$^{Cre/+}$*Egfr*$^{fl/fl}$ mice compared with the control mice (Fig. 3A). To confirm whether Egfr modulates MCP-1 production, we silenced *Egfr* in ECs. ECs produced high levels of MCP-1 after *Egfr* knockdown (Fig. 3B). Furthermore, we measured *IL8*, *ICAM1*, and *VCAM1* by quantitative PCR (Supplemental Fig. 4A) and flow cytometry (Supplemental Fig. 4B) after *EGFR* knockdown in human hepatic ECs. We observed that *Il8* mRNA and VCAM-1 protein levels were diminished after *EGFR* silencing. Using Ingenuity Pathway Analysis, we identified 20 transcription factors, which are regulated by EGFR and may control MCP-1 production (Supplemental Fig. 4C). Transcription factors, such as STAT3, EGR1, KLF6, STAT1, and SMAD3, were upregulated upon *EGFR* silencing in the absence (Supplemental Fig. 4D) and presence (Supplemental Fig. 4E) of palmitate. SMAD4, SP1, and NPM1 were uniquely elevated in the presence of palmitate after si*EGFR* treatment. This suggests that disrupted hepatic endothelial Egfr signaling unleashes MCP-1 production, resulting in monocyte recruitment and macrophage differentiation. To test this hypothesis, we performed parabiosis between GFP$^+$ and *Cdh5*$^{Cre/+}$*Egfr*$^{fl/fl}$ or *Cdh5*$^{+/+}$*Egfr*$^{fl/fl}$ mice fed with a high-fat diet (Fig. 3C). Parabiosis experiments help to delineate monocyte recruitment from the blood. Parabiont-derived GFP$^+$ macrophages, both monocyte-derived macrophages and Kupffer cells, accumulated in a higher quantity in the liver of *Cdh5*$^{Cre/+}$ *Egfr*$^{fl/fl}$ mice compared with littermate control (Fig. 3D, 3E). Confocal microscopy confirmed higher abundance of GFP$^+$ hepatic macrophages in the obese parabionts lacking *Egfr* in ECs (Supplemental Fig. 4F). These macrophages were located near hepatic sinusoidal ECs in *Cdh5*$^{Cre/+}$*Egfr*$^{fl/fl}$ parabionts. We also observed increases in recruited splenic monocyte and macrophage numbers (Supplemental Fig. 4G). In summary, these data indicate that the deficiency of *Egfr* in hepatic

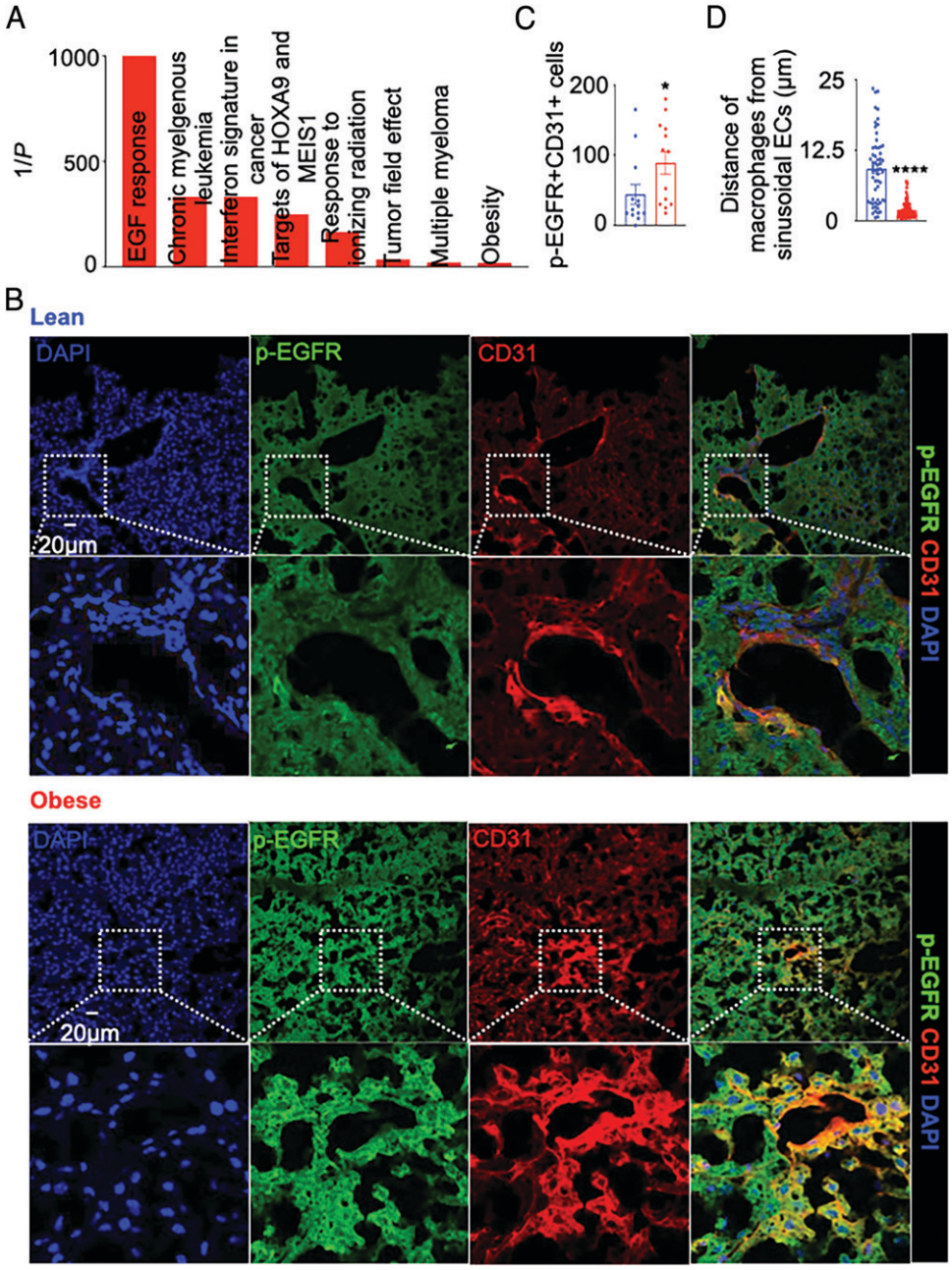

FIGURE 1. Type II diabetes increases p-EGFR in hepatic sinusoidal ECs. (**A**) Pathway analysis of the genes differentially expressed in ECs of diabetic versus nondiabetic mice. $1/p$ indicates the inverse values of the probability that the null hypotheses are true. (**B**) Representative immunofluorescence images and quantification of p-EGFR staining in hepatic sinusoidal ECs in lean (fed with a chow diet) and obese (fed with a high-fat diet) mice. The bar graphs depict the quantification of p-EGFR$^+$ ECs (**C**, technical replicates from $n = 5$ mice) and distance of F4/80$^+$ macrophages from the sinusoids (**D**, technical replicates from $n = 5$ mice) using immunofluorescence microscopy in lean and obese mice. Each data point in (C) and (D) represents a field of view. The data in (A) are obtained from one microarray experiment, whereas the data shown in (B)–(D) are pooled from two different experiments. $n = 5$ per group. Data are mean ± SEM. $*p < 0.05$, $****p < 0.0001$.

sinusoidal ECs results in a heightened amount of MCP-1, leading to hepatic monocyte accumulation and macrophage differentiation.

Accumulation of hepatic macrophages in EC-specific Egfr*-deficient mice leads to glucose intolerance*

To explore the contributions of MCP-1 in glucose intolerance in *Cdh5*$^{Cre/+}$*Egfr*$^{fl/fl}$ mice, we neutralized this chemokine in obese mice lacking endothelial *Egfr* (Fig. 4A). This resulted in a decreased number of hepatic monocyte-derived macrophages and Kupffer cells compared with the isotype Ab-treated control group (Fig. 4B, 4C). In addition, the livers of these mice harbored diminished numbers of total monocytes, and Ly-6C^{low} and Ly-6C^{hi} monocytes, indicating disruption of monocyte recruitment into the liver after MCP-1 neutralization and thereby reduced macrophage production. Interestingly, we observed augmented frequencies and numbers of monocytes in the bone marrow after MCP-1 neutralization (Fig. 4D), confirming the role of MCP-1 in monocyte egress from the bone marrow niche (32). Concomitantly, MCP-1 neutralization also improved glucose clearance in diabetic *Cdh5*$^{Cre/+}$*Egfr*$^{fl/fl}$ mice (Fig. 4E, 4F). In line with improved glucose and insulin tolerance in *Cdh5*$^{Cre/+}$*Egfr*$^{fl/fl}$ mice after MCP-1 neutralization, systemic insulin concentrations lessened (Fig. 4G), whereas serum fatty acids,

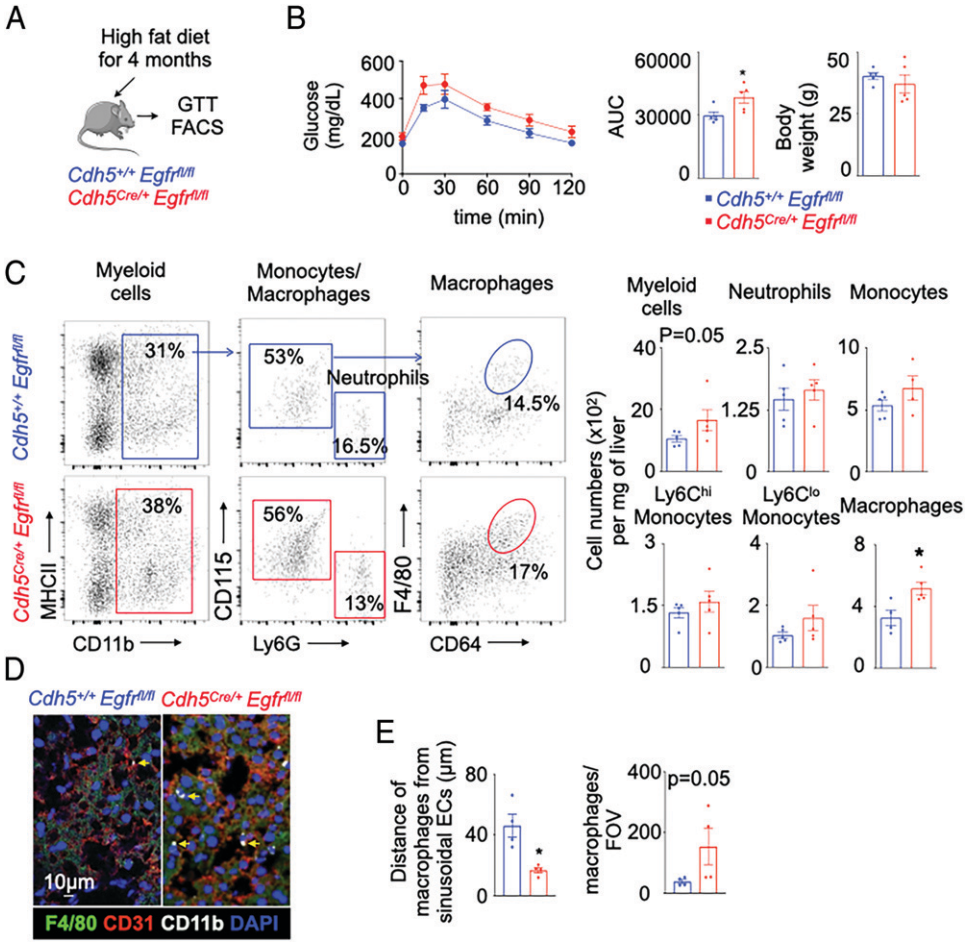

FIGURE 2. EC-specific *Egfr* deletion enhances glucose intolerance and hepatic monocyte recruitment. (**A**) Schematic representation of the experimental design. (**B**) GTT and body weights in the mice lacking endothelial *Egfr* compared with the littermate controls after 4 mo of high-fat-diet feeding. (**C**) Representative flow cytometric plots and gating strategies of hepatic myeloid cells in obese $Cdh5^{Cre/+}Egfr^{fl/fl}$ and control mice. The bar graphs depict quantification of hepatic myeloid cells, neutrophils, monocytes, Ly-6C^{high} monocytes, Ly-6C^{low} monocytes, and macrophages. (**D**) Representative immunofluorescence images of hepatic macrophages in the obese mice. The arrows indicate the macrophages. (**E**) The distance of macrophages (CD11b$^+$F4/80$^+$) to hepatic sinusoidal ECs and number of macrophages per field of view (FOV) have been calculated. $n = 4–5$ per group. The data are obtained from one experiment. Data are mean ± SEM. $^*p < 0.05$.

glycerol, and body weights were unchanged (Fig. 4H). In aggregate, these data strongly support the hypothesis that MCP-1 produced in response to endothelial deficiency of *Egfr* recruits monocytes and promotes macrophage abundance in the liver, exacerbating glucose intolerance in obesity.

Hepatic macrophage depletion ameliorates glucose intolerance

To specifically investigate whether hepatic macrophages play a crucial role in triggering glucose intolerance, we depleted these macrophages by $GdCl_3$ in obese $Cdh5^{Cre/+}$ $Egfr^{fl/fl}$ and littermate control mice (34) (Fig. 5A). This injection resulted in a significantly reduced number of Kupffer cells and monocyte-derived macrophages (Fig. 5B, 5C). Interestingly, hepatic macrophages distanced themselves from the sinusoids after $GdCl_3$ injection. $Cdh5^{Cre/+}$ $Egfr^{fl/fl}$ mice, after hepatic macrophage depletion, exhibited significantly improved glucose tolerance compared with control $Cdh5^{Cre/+}$ $Egfr^{fl/fl}$ mice as determined by a GTT (Fig. 5D). However, the ITT did not exhibit any significant difference in insulin sensitivity (Fig. 5E). In line with improved glucose tolerance, GdCl3-treated mice had lower systemic insulin levels (Fig. 5F). However, the serum concentrations of fatty acids (Fig. 5G), glycerol (Fig. 5H), and triglycerides (Fig. 5I) did not alter after GdCl3 treatment.

Discussion

In this article, we reveal that type II diabetes alters Egfr signaling in hepatic sinusoidal ECs. Disrupted endothelial Egfr led to augmented hepatic monocyte recruitment and macrophage differentiation via MCP-1. This accumulation of hepatic macrophages in EC-specific *Egfr*-deficient mice contributed to glucose intolerance (Fig. 5J). Our results demonstrate a novel mechanism of the maintenance of glucose tolerance by Egfr signaling in hepatic ECs.

Endothelial Egfr signaling has been found to regulate the progression of various diseases, such as atherosclerosis and type II diabetes (35, 36). Especially, several preclinical studies have shown that the Egfr signaling plays an essential role in diabetes-induced cardiac dysfunction and chronic kidney disease (37, 38). Considering these reports together with enriched Egfr expression in hepatic sinusoidal ECs in the setting of type II diabetes, we assumed metabolic dysfunctions in mice lacking this receptor in ECs. As expected, we observed an increased number of hepatic myeloid cells, especially

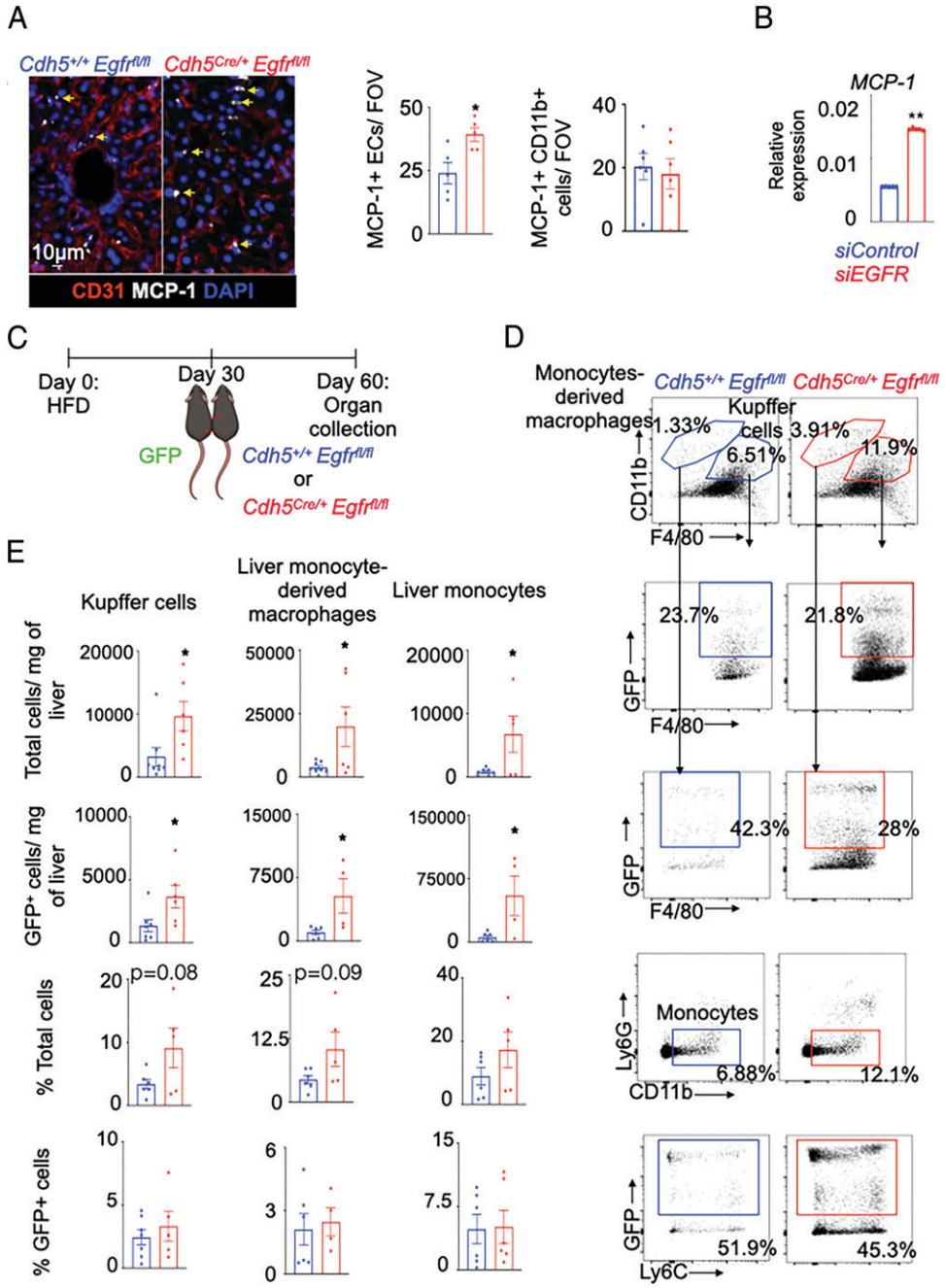

FIGURE 3. Disrupted endothelial Egfr signaling promotes monocyte recruitment into the liver via Mcp-1. (**A**) Representative immunofluorescence images of Mcp-1 staining in hepatic ECs in diabetic $Cdh5^{Cre/+}Egfr^{fl/fl}$ and control mice. MCP-1$^+$ ECs and monocytes were quantified. (**B**) *Egfr* was silenced in ECs, and the expression of *Mcp-1* was quantified by quantitative PCR. (**C**) Parabiosis between GFP$^+$ and either $Cdh5^{Cre/+}Egfr^{fl/fl}$ or $Cdh5^{+/+}Egfr^{fl/fl}$ mice (both GFP$^-$) fed with a high-fat diet was performed. (**D**) Representative flow cytometric plots and gating strategies of hepatic myeloid cells in the GFP$^-$ parabionts. (**E**) The bar graphs show quantification of different myeloid cell subtypes in the liver. $n = 4–7$ per group. The data are obtained from two experiments. Data are mean ± SEM. $^*p < 0.05$, $^{**}p < 0.01$.

macrophages, and systemic glucose intolerance in $Cdh5^{Cre/+}Egfr^{fl/fl}$ mice compared with wild type mice with type II diabetes. Augmented monocyte supply and macrophage accumulation in obese $Cdh5^{Cre/+}Egfr^{fl/fl}$ mice are therefore likely responsible for type II diabetes exacerbation. These findings are congruent with the observations that hepatic ECs are crucial to inflammatory nonalcoholic steatohepatitis (39–41). In contrast with these observations, a recent study (42) showed that inhibition of Egfr activation is associated with ameliorated diabetic nephropathy and insulin resistance in type II diabetes. This discordant finding can be explained in two ways. First, the difference could be caused by the cell type–specific role of Egfr. This study shows that endothelial Egfr dampens hepatic inflammation by suppressing monocyte recruitment. In contrast, a study (43) has shown that leukocyte Egfr is responsible for their infiltration in tissue space. Thus, the beneficial effects as a result of the deficiency of Egfr in leukocytes may overcome the detrimental role of Egfr deletion in ECs in mice lacking this receptor globally. Second, as discussed in a review paper (44), a physiological range of Egfr signaling is essential to maintain homeostasis. Hepatocyte-specific HB-EGF gene deletion and overexpression induced inflammation and fibrosis of the liver.

We observed that *Egfr* deficiency not only increased the number of monocyte-derived macrophages but also Kupffer cells in the

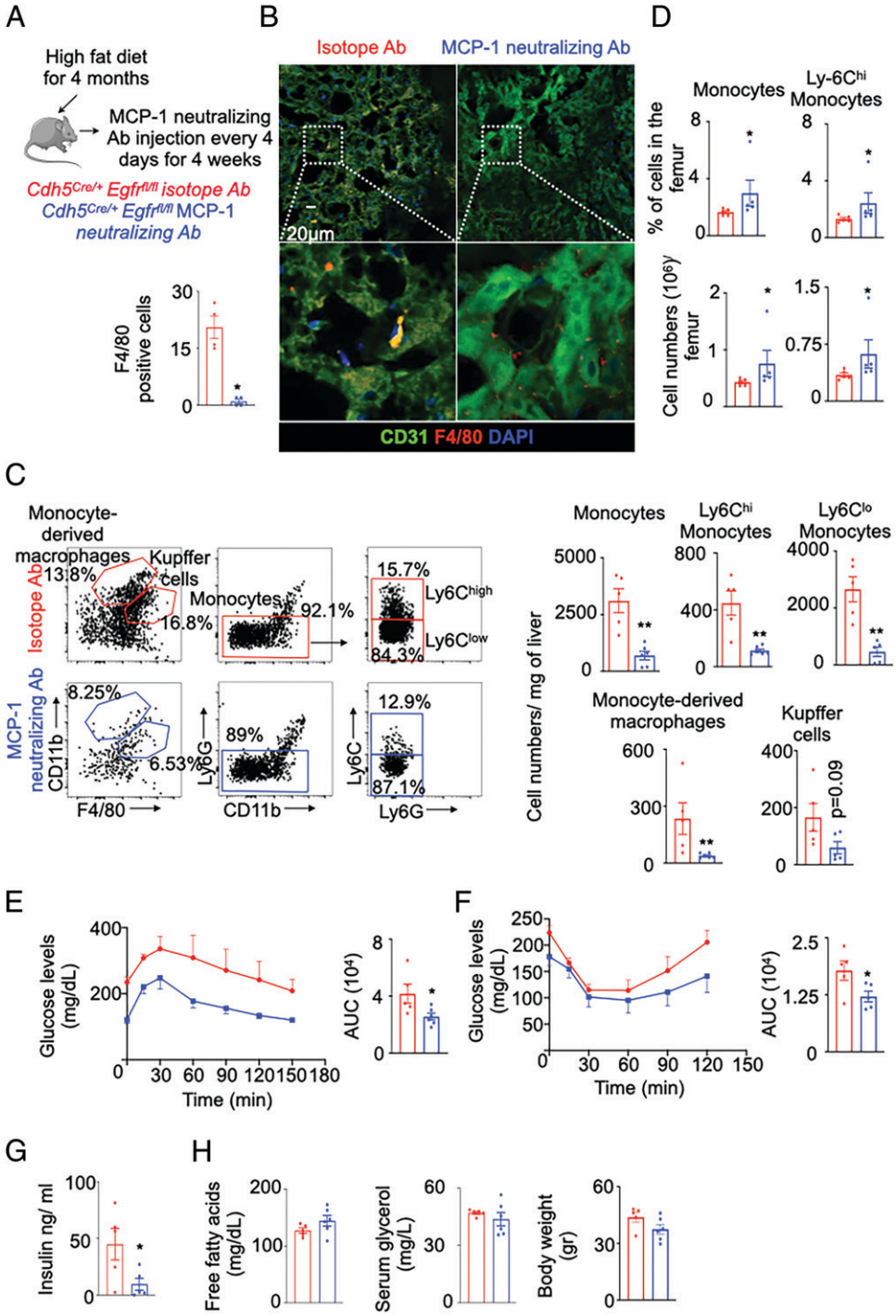

FIGURE 4. Accumulation of hepatic macrophages in EC-specific *Egfr*-deficient obese mice leads to glucose intolerance. (**A**) Schematic representation of the experiment neutralizing MCP-1 in obese mice lacking endothelial *Egfr*. (**B**) F4/80 and CD31 staining was performed to ensure the effectiveness of MCP-1 neutralization. (**C**) Representative flow cytometric plots showing hepatic monocyte-derived macrophages and Kupffer cells in the mice after MCP-1 neutralization. Flow cytometry was employed to quantify bone marrow myeloid cell numbers and frequencies (**D**). GTT (**E**) and ITT (**F**) were performed in obese $Cdh5^{Cre/+}Egfr^{fl/fl}$ mice after isotype or MCP-1 neutralizing Ab treatment. GTT and ITT data were analyzed using one-tailed *t* test. Systemic insulin concentrations (**G**), fatty acids, glycerol, and body weights (**H**) were measured in these mice. $n = 5–6$ per group. The data are obtained from two experiments. Data are mean ± SEM. $^*p < 0.05$, $^{**}p < 0.01$.

liver. These data indicate that recruited monocytes can also differentiate into Kupffer cells. Consistently, Mcp-1 neutralization, which blocked monocyte influx into the liver, also lowered the Kupffer cell content. There are mainly two subtypes of liver macrophages, monocyte-derived macrophages and Kupffer cells, which share many transcriptomic and functional features, regardless of their origin (45). Studies have reported that monocytes could give rise to self-renewing Kupffer cells when the niche is available (46). *Egfr* deficiency also increased MCP-1 expression in mouse hepatic sinusoidal ECs in vivo and human ECs in vitro. As we know, MCP-1 is anchored in the membrane of ECs by glycosaminoglycan side chains of proteoglycans and exhibits a chemotactic activity for monocytes (47). We therefore hypothesized that augmented monocyte recruitment and macrophage differentiation in the liver of

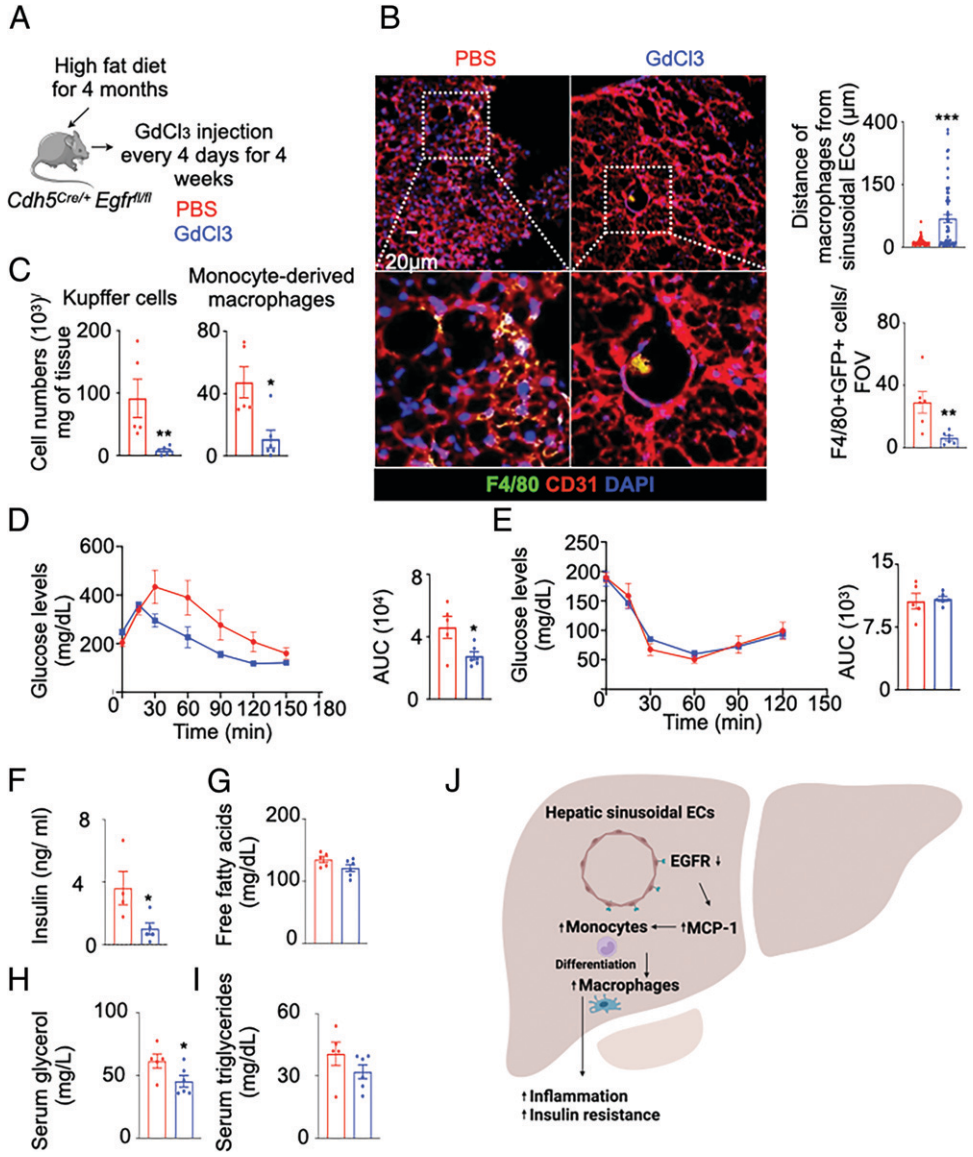

FIGURE 5. Hepatic macrophage depletion ameliorates glucose intolerance. (**A**) Schematic representation of the experimental design. Hepatic macrophages were depleted by $GdCl_3$ in obese *Cdh5*$^{Cre/+}$*Egfr*$^{fl/fl}$ mice. (**B**) Representative immunofluorescence images and quantification of hepatic macrophages after $GdCl_3$ injection. Each data point represents a field of view from $n = 5$ mice per group. (**C**) Quantification of Kupffer cells and liver monocyte-derived macrophages by flow cytometry after $GdCl_3$ injection. GTT (**D**) and ITT (**E**) were performed, and GTT experimental data were analyzed using one-tailed *t* test. The concentrations of systemic insulin (**F**), fatty acids (**G**), glycerol (**H**), and triglycerides (**I**) were evaluated after hepatic macrophage depletion. (**J**) The schema depicts the mechanisms of insulin resistance in the absence of endothelial EGFR. $n = 4–6$ per group. The data are obtained from two experiments. Data are mean ± SEM. $*p < 0.05$, $**p < 0.01$, $***p < 0.001$.

diabetic *Cdh5*$^{Cre/+}$*Egfr*$^{fl/fl}$ mice is induced via MCP-1. Consistently, we found that MCP-1 neutralization in *Cdh5*$^{Cre/+}$*Egfr*$^{fl/fl}$ mice resulted in a decreased number of hepatic monocyte-derived macrophages and Kupffer cells. This resulted in improved glucose tolerance compared with the isotype Ab-treated control group. *Cdh5*$^{Cre/+}$*Egfr*$^{fl/fl}$ mice after hepatic macrophage depletion also showed markedly less glucose intolerance compared with control Ab-injected *Cdh5*$^{Cre/+}$*Egfr*$^{fl/fl}$ mice. Although insulin levels decreased after $GdCl_3$ treatment, an ITT test did not display any difference compared with PBS-injected mice. This could be because of the effect of $GdCl_3$ on the pancreas, resulting in reduced insulin secretion. Similarly, this study does not examine whether MCP-1 neutralization affects macrophages in the pancreas, resulting in suppressed insulin production. Future studies will be required to discern these possibilities.

Overall, the data presented in this article support an insulin-sensitizing role of hepatic endothelial Egfr signaling by suppressing excessive monocyte recruitment and macrophage differentiation. However, we cannot rule out the contribution of exaggerated monocyte cell production by the bone marrow in the absence of endothelial Egfr in type II diabetes exacerbation. In fact, Egfr deficiency in bone marrow ECs increased proliferation and differentiation of myeloid progenitors, resulting in monocytosis (29). Discerning the role of bone marrow versus hepatic EC-specific Egfr in type II diabetes is beyond the scope of this study because organ-specific cre recombinase mice will be required.

Several questions remain unanswered. We do not know the ligand(s) responsible for Egfr-mediated protection against inflammation and glucose intolerance. Egfr can interact with several ligands, including amphiregulin, TGF-α, and heparin-binding EGF (48). Interaction with these various ligands may result in different Egfr signaling, resulting in different physiological responses. Future studies will be required to examine this.

Acknowledgments

We acknowledge the National Institutes of Health–supported microscopy resources in the Center for Biologic Imaging, University of Pittsburgh, School of Medicine. The figures were designed using BioRender software.

Disclosures

The authors have no financial conflicts of interest.

References

1. International Diabetes Federation. 2019. *IDF Diabetes Atlas*, 9th Ed, Brussels, Belgium.
2. Stratton, I. M., A. I. Adler, H. A. Neil, D. R. Matthews, S. E. Manley, C. A. Cull, D. Hadden, R. C. Turner, and R. R. Holman. 2000. Association of glycaemia with macrovascular and microvascular complications of type 2 diabetes (UKPDS 35): prospective observational study. *BMJ* 321: 405–412.
3. Holman, R. R., S. K. Paul, M. A. Bethel, D. R. Matthews, and H. A. W. Neil. 2008. 10-year follow-up of intensive glucose control in type 2 diabetes. *N. Engl. J. Med.* 359: 1577–1589.
4. DeFronzo, R. A., E. Ferrannini, L. Groop, R. R. Henry, W. H. Herman, J. J. Holst, F. B. Hu, C. R. Kahn, I. Raz, G. I. Shulman, et al. 2015. Type 2 diabetes mellitus. *Nat. Rev. Dis. Primers* 1: 15019.
5. Romeo, G. R., J. Lee, and S. E. Shoelson. 2012. Metabolic syndrome, insulin resistance, and roles of inflammation—mechanisms and therapeutic targets. *Arterioscler. Thromb. Vasc. Biol.* 32: 1771–1776.
6. Arkan, M. C., A. L. Hevener, F. R. Greten, S. Maeda, Z.-W. Li, J. M. Long, A. Wynshaw-Boris, G. Poli, J. Olefsky, and M. Karin. 2005. IKK-beta links inflammation to obesity-induced insulin resistance. *Nat. Med.* 11: 191–198.
7. de Alvaro, C., T. Teruel, R. Hernandez, and M. Lorenzo. 2004. Tumor necrosis factor alpha produces insulin resistance in skeletal muscle by activation of inhibitor kappaB kinase in a p38 MAPK-dependent manner. *J. Biol. Chem.* 279: 17070–17078.
8. Brownlee, M. 2005. The pathobiology of diabetic complications: a unifying mechanism. *Diabetes* 54: 1615–1625.
9. Giacco, F., and M. Brownlee. 2010. Oxidative stress and diabetic complications. *Circ. Res.* 107: 1058–1070.
10. Lumeng, C. N., and A. R. Saltiel. 2011. Inflammatory links between obesity and metabolic disease. *J. Clin. Invest.* 121: 2111–2117.
11. Nishimura, S., I. Manabe, M. Nagasaki, K. Eto, H. Yamashita, M. Ohsugi, M. Otsu, K. Hara, K. Ueki, S. Sugiura, et al. 2009. CD8+ effector T cells contribute to macrophage recruitment and adipose tissue inflammation in obesity. *Nat. Med.* 15: 914–920.
12. Bertola, A., T. Ciucci, D. Rousseau, V. Bourlier, C. Duffaut, S. Bonnafous, C. Blin-Wakkach, R. Anty, A. Iannelli, J. Gugenheim, et al. 2012. Identification of adipose tissue dendritic cells correlated with obesity-associated insulin-resistance and inducing Th17 responses in mice and patients. *Diabetes* 61: 2238–2247.
13. Feuerer, M., L. Herrero, D. Cipolletta, A. Naaz, J. Wong, A. Nayer, J. Lee, A. B. Goldfine, C. Benoist, S. Shoelson, and D. Mathis. 2009. Lean, but not obese, fat is enriched for a unique population of regulatory T cells that affect metabolic parameters. *Nat. Med.* 15: 930–939.
14. Perry, R. J., J. G. Camporez, R. Kursawe, P. M. Titchenell, D. Zhang, C. J. Perry, M. J. Jurczak, A. Abudukadier, M. S. Han, X.-M. Zhang, et al. 2015. Hepatic acetyl CoA links adipose tissue inflammation to hepatic insulin resistance and type 2 diabetes. *Cell* 160: 745–758.
15. Leclercq, I. A., A. Da Silva Morais, B. Schroyen, N. Van Hul, and A. Geerts. 2007. Insulin resistance in hepatocytes and sinusoidal liver cells: mechanisms and consequences. *J. Hepatol.* 47: 142–156.
16. Rask-Madsen, C., and G. L. King. 2007. Mechanisms of disease: endothelial dysfunction in insulin resistance and diabetes. *Nat. Clin. Pract. Endocrinol. Metab.* 3: 46–56.
17. Schalkwijk, C. G., and C. D. A. Stehouwer. 2005. Vascular complications in diabetes mellitus: the role of endothelial dysfunction. *Clin. Sci. (Lond.)* 109: 143–159.
18. Amin, D. N., K. Hida, D. R. Bielenberg, and M. Klagsbrun. 2006. Tumor endothelial cells express epidermal growth factor receptor (EGFR) but not ErbB3 and are responsive to EGF and to EGFR kinase inhibitors. *Cancer Res.* 66: 2173–2180.
19. Gao, P., X.-M. Wang, D.-H. Qian, Z.-X. Qin, J. Jin, Q. Xu, Q.-Y. Yuan, X.-J. Li, and L.-Y. Si. 2013. Induction of oxidative stress by oxidized LDL via meprinα-activated epidermal growth factor receptor in macrophages. *Cardiovasc. Res.* 97: 533–543.
20. Zhang, H., D. Chalothorn, L. F. Jackson, D. C. Lee, and J. E. Faber. 2004. Transactivation of epidermal growth factor receptor mediates catecholamine-induced growth of vascular smooth muscle. *Circ. Res.* 95: 989–997.
21. Li, W., Q. Fang, P. Zhong, L. Chen, L. Wang, Y. Zhang, J. Wang, X. Li, Y. Wang, J. Wang, and G. Liang. 2016. EGFR inhibition blocks palmitic acid-induced inflammation in cardiomyocytes and prevents hyperlipidemia-induced cardiac injury in mice. *Sci. Rep.* 6: 24580.
22. Wee, P., and Z. Wang. 2017. Epidermal growth factor receptor cell proliferation signaling pathways. *Cancers (Basel)* 9: 52.
23. Shang, D., D. Sun, C. Shi, J. Xu, M. Shen, X. Hu, H. Liu, and Z. Tu. 2020. Activation of epidermal growth factor receptor signaling mediates cellular senescence induced by certain pro-inflammatory cytokines. *Aging Cell* 19: e13145.
24. Carlin, C. R. 2022. Role of EGF receptor regulatory networks in the host response to viral infections. *Front. Cell. Infect. Microbiol.* 11: 820355.
25. Yarden, Y. 2001. The EGFR family and its ligands in human cancer. signalling mechanisms and therapeutic opportunities. *Eur. J. Cancer* 37(Suppl. 4): 3–8.
26. Makinoshima, H., M. Takita, S. Matsumoto, A. Yagishita, S. Owada, H. Esumi, and K. Tsuchihara. 2014. Epidermal growth factor receptor (EGFR) signaling regulates global metabolic pathways in EGFR-mutated lung adenocarcinoma. *J. Biol. Chem.* 289: 20813–20823.
27. Sheng, L., G. Bayliss, and S. Zhuang. 2021. Epidermal growth factor receptor: a potential therapeutic target for diabetic kidney disease. *Front. Pharmacol.* 11: 598910.
28. Zhang, M.-Z., Y. Wang, P. Paueksakon, and R. C. Harris. 2014. Epidermal growth factor receptor inhibition slows progression of diabetic nephropathy in association with a decrease in endoplasmic reticulum stress and an increase in autophagy. *Diabetes* 63: 2063–2072.
29. Hoyer, F. F., X. Zhang, E. Coppin, S. B. Vasamsetti, G. Modugu, M. J. Schloss, D. Rohde, C. S. McAlpine, Y. Iwamoto, P. Libby, et al. 2020. Bone marrow endothelial cells regulate myelopoiesis in diabetes mellitus. *Circulation* 142: 244–258.
30. Korenblat, K. M., E. Fabbrini, B. S. Mohammed, and S. Klein. 2008. Liver, muscle, and adipose tissue insulin action is directly related to intrahepatic triglyceride content in obese subjects. *Gastroenterology* 134: 1369–1375.
31. Kanter, J. E., F. Kramer, S. Barnhart, M. M. Averill, A. Vivekanandan-Giri, T. Vickery, L. O. Li, L. Becker, W. Yuan, A. Chait, et al. 2012. Diabetes promotes an inflammatory macrophage phenotype and atherosclerosis through acyl-CoA synthetase 1. *Proc. Natl. Acad. Sci. USA* 109: E715–E724.
32. Shi, C., T. Jia, S. Mendez-Ferrer, T. M. Hohl, N. V. Serbina, L. Lipuma, I. Leiner, M. O. Li, P. S. Frenette, and E. G. Pamer. 2011. Bone marrow mesenchymal stem and progenitor cells induce monocyte emigration in response to circulating toll-like receptor ligands. *Immunity* 34: 590–601.
33. Gerszten, R. E., E. A. Garcia-Zepeda, Y. C. Lim, M. Yoshida, H. A. Ding, M. A. Gimbrone, Jr., A. D. Luster, F. W. Luscinskas, and A. Rosenzweig. 1999. MCP-1 and IL-8 trigger firm adhesion of monocytes to vascular endothelium under flow conditions. *Nature* 398: 718–723.
34. Joseph, B., H. Malhi, K. K. Bhargava, C. J. Palestro, R. S. McCuskey, and S. Gupta. 2002. Kupffer cells participate in early clearance of syngeneic hepatocytes transplanted in the rat liver. *Gastroenterology* 123: 1677–1685.
35. Zeboudj, L., A. Giraud, L. Guyonnet, Y. Zhang, L. Laurans, B. Esposito, J. Vilar, A. Chipont, N. Papac-Milicevic, C. J. Binder, et al. 2018. Selective EGFR (epidermal growth factor receptor) deletion in myeloid cells limits atherosclerosis. *Arterioscler. Thromb. Vasc. Biol.* 38: 114–119.
36. Song, N. -J., A. Lee, R. Yasmeen, Q. Shen, K. Yang, S. B. Kumar, D. Muhanna, S. Arnipalli, S. F. Noria, B. J. Needleman, et al. 2022. Epiregulin as an alternative ligand for leptin receptor alleviates glucose intolerance without change in obesity. *Cells* 11: 425.
37. Akhtar, S., and I. F. Benter. 2013. The role of epidermal growth factor receptor in diabetes-induced cardiac dysfunction. *Bioimpacts* 3: 5–9.
38. Rayego-Mateos, S., R. Rodrigues-Diez, J. L. Morgado-Pascual, F. Valentijn, J. M. Valdivielso, R. Goldschmeding, and M. Ruiz-Ortega. 2018. Role of epidermal growth factor receptor (EGFR) and its ligands in kidney inflammation and damage. *Mediators Inflamm.* 2018: 8739473.
39. Miyao, M., H. Kotani, T. Ishida, C. Kawai, S. Manabe, H. Abiru, and K. Tamaki. 2015. Pivotal role of liver sinusoidal endothelial cells in NAFLD/NASH progression. *Lab. Invest.* 95: 1130–1144.
40. Miyachi, Y., K. Tsuchiya, C. Komiya, K. Shiba, N. Shimazu, S. Yamaguchi, M. Deushi, M. Osaka, K. Inoue, Y. Sato, et al. 2017. Roles for cell-cell adhesion and contact in obesity-induced hepatic myeloid cell accumulation and glucose intolerance. *Cell Rep.* 18: 2766–2779.
41. McCuskey, R. S., Y. Ito, G. R. Robertson, M. K. McCuskey, M. Perry, and G. C. Farrell. 2004. Hepatic microvascular dysfunction during evolution of dietary steatohepatitis in mice. *Hepatology* 40: 386–393.
42. Li, Z., Y. Li, J. M. Overstreet, S. Chung, A. Niu, X. Fan, S. Wang, Y. Wang, M.-Z. Zhang, and R. C. Harris. 2018. Inhibition of epidermal growth factor receptor activation is associated with improved diabetic nephropathy and insulin resistance in type 2 diabetes. *Diabetes* 67: 1847–1857.
43. Aupperlee, M. D., Y. Zhao, Y. S. Tan, J. R. Leipprandt, J. Bennett, S. Z. Haslam, and R. C. Schwartz. 2014. Epidermal growth factor receptor (EGFR) signaling is a key mediator of hormone-induced leukocyte infiltration in the pubertal female mammary gland. *Endocrinology* 155: 2301–2313.
44. Kim, S., V. Subramanian, A. Abdel-Latif, and S. Lee. 2020. Role of heparin-binding epidermal growth factor-like growth factor in oxidative stress-associated metabolic diseases. *Metab. Syndr. Relat. Disord.* 18: 186–196.
45. Beattie, L., A. Sawtell, J. Mann, T. C. M. Frame, B. Teal, F. de Labastida Rivera, N. Brown, K. Walwyn-Brown, J. W. J. Moore, S. MacDonald, et al. 2016. Bone marrow-derived and resident liver macrophages display unique transcriptomic signatures but similar biological functions. *J. Hepatol.* 65: 758–768.
46. Scott, C. L., F. Zheng, P. De Baetselier, L. Martens, Y. Saeys, S. De Prijck, S. Lippens, C. Abels, S. Schoonooghe, G. Raes, et al. 2016. Bone marrow-derived monocytes give rise to self-renewing and fully differentiated Kupffer cells. *Nat. Commun.* 7: 10321.
47. Yoshimura, T. 2018. The chemokine MCP-1 (CCL2) in the host interaction with cancer: a foe or ally? *Cell. Mol. Immunol.* 15: 335–345.
48. Wieduwilt, M. J., and M. M. Moasser. 2008. The epidermal growth factor receptor family: biology driving targeted therapeutics. *Cell. Mol. Life Sci.* 65: 1566–1584.